Inorg. Chem. **2003**, *42*, 8606–8608

Synthesis, Characterization, and Dioxygen Reactivity of Tetracarboxylate-Bridged Diiron(II) Complexes with Coordinated Substrates

Sungho Yoon and Stephen J. Lippard*

Department of Chemistry, Massachusetts Institute of Technology, Cambridge, Massachusetts 02139

Received August 28, 2003

The synthesis and characterization of $[Fe_2(\mu\text{-}O_2CAr^{Tol})_4L_2]$ complexes, where L is benzylamine or 4-methoxybenzylamine (BA^{p-OMe}), are described. The reaction of the latter diiron(II) complex with dioxygen at −78 °C affords a metastable mixed-valent Fe(II)-Fe(III) green intermediate. When O_2 is introduced at ambient temperature, *N*-dealkyation occurs to yield anisaldehyde, eliminating *N*-oxidation as a viable pathway for the reaction. Use of $[Fe_2(\mu\text{-}O_2CAr^{Tol})_4(\alpha\text{-}d_1\text{-}BA^{p-OMe})_2]$ allowed a deuterium kinetic isotope of ∼3 to be determined.

Dioxygen activation and O-atom transfer reactions promoted by iron- and copper-containing metalloenzymes are of considerable current interest. Monooxygenases,[1−3] which catalyze the hydroxylation of unactivated hydrocarbons, are of particular interest because of their ability to hydroxylate methyl groups bearing a range of substituents.[4] The hydroxylase component of soluble methane monooxygenase (MMOH) performs this function by first activating dioxygen to afford reactive intermediate(s).[5] The resulting oxidant can insert one oxygen atom selectively into a C−H bond. Understanding this remarkable process in molecular detail is an important objective which, if accomplished, could both reveal how the metalloproteins work and facilitate the design of catalysts for O_2 activation and selective hydrocarbon oxidation.

In pursuit of our goal to prepare diiron(II) complexes that mimic the functional chemistry of MMOH, we reported the carboxylate-bridged diiron(II) complex, $[Fe_2(\mu\text{-}O_2CAr^{Tol})_2(O_2CAr^{Tol})_2(N,N\text{-}Bn_2en)_2]$, where $Ar^{Tol}CO_2^-$ is 2,6-di(*p*-tolyl)-benzoate and *N*,*N*-Bn_2en is *N*,*N*-dibenzylethylenediamine,

Scheme 1

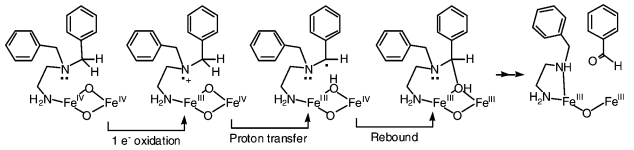

which oxidatively *N*-dealkylates a tethered *N*-benzylamino functionality upon reaction with dioxygen.[6,7] One of the proposed reaction pathways was sequential one-electron oxidation of the nitrogen atom by a putative diiron(IV) oxo intermediate, followed by α-proton abstraction and oxygen rebound (Scheme 1). This possibility was suggested by the proximity of the lone pair electrons on the uncoordinated nitrogen atom of the Bn_2en ligand to the proposed high-valent intermediate and by the precedence for such chemistry in heme iron oxidations.[8] In order to test this mechanism, we devised a system to achieve *N*-dealkylation under similar conditions but which lacks the nonbonded electron pair of the uncoordinated *N*-benzylamino group.

In the present report we describe the synthesis and characterization of $[Fe_2(\mu\text{-}O_2CAr^{Tol})_4L_2]$ complexes, where L is benzylamine (BA) or 4-methoxybenzylamine (BA^{p-OMe}), and the reactions of the latter with dioxygen (Scheme 2). Addition of 2 equiv of BA or BA^{p-OMe} to $[Fe_2(\mu\text{-}O_2CAr^{Tol})_2(O_2CAr^{Tol})_2(THF)_2]$[9] in CH_2Cl_2 afforded the tetracarboxylate-bridged diiron(II) complexes $[Fe_2(\mu\text{-}O_2CAr^{Tol})_4(BA)_2]$ (**1**) and $[Fe_2(\mu\text{-}O_2CAr^{Tol})_4(BA^{p-OMe})_2]$ (**2**), respectively. Structural characterization of both compounds by X-ray crystallography revealed Fe···Fe distances and square pyramidal coordination geometry that closely resemble those of previously reported diiron(II) paddlewheel complexes (Table 1; Figures 1 and S1).[10,11] The N-donor ligands are

* Corresponding author. E-mail: lippard@lippard.mit.edu.

(1) Solomon, E. I.; Brunold, T. C.; Davis, M. I.; Kemsley, J. N.; Lee, S.-K.; Lehnert, N.; Neese, F.; Skulan, A. J.; Yang, Y.-S.; Zhou, J. *Chem. Rev.* **2000**, *100*, 235−349.
(2) Feig, A. L.; Lippard, S. J. *Chem. Rev.* **1994**, *94*, 759−805.
(3) Solomon, E. I.; Sundaram, U. M.; Machonkin, T. E. *Chem. Rev.* **1996**, *96*, 2563−2605.
(4) Ambundo, E. A.; Friesner, R. A.; Lippard, S. J. *J. Am. Chem. Soc.* **2002**, *124*, 8770−8771 and references cited therein.
(5) Merkx, M.; Kopp, D. A.; Sazinsky, M. H.; Blazyk, J. L.; Müller, J.; Lippard, S. J. *Angew. Chem., Int. Ed.* **2001**, *40*, 2782−2807.
(6) Lee, D.; Lippard, S. J. *Inorg. Chem.* **2002**, *41*, 827−837.
(7) Lee, D.; Lippard, S. J. *J. Am. Chem. Soc.* **2001**, *123*, 4611−4612.
(8) Sono, M.; Roach, M. P.; Coulter, E. D.; Dawson, J. H. *Chem. Rev.* **1996**, *96*, 2841−2887.
(9) Lee, D.; Lippard, S. J. *Inorg. Chem.* **2002**, *41*, 2704−2719.
(10) Lee, D.; Du Bois, J.; Petasis, D.; Hendrich, M. P.; Krebs, C.; Huynh, B. H.; Lippard, S. J. *J. Am. Chem. Soc.* **1999**, *121*, 9893−9894.
(11) Chavez, F. A.; Ho, R. Y. N.; Pink, M.; Young, V. G., Jr.; Kryatov, S. V.; Rybak-Akimova, E. V.; Andres, H.; Münck, E.; Que, L., Jr.; Tolman, W. B. *Angew. Chem., Int. Ed.* **2002**, *41*, 149−152.

10.1021/ic0350133 CCC: $25.00
Published on Web 11/26/2003

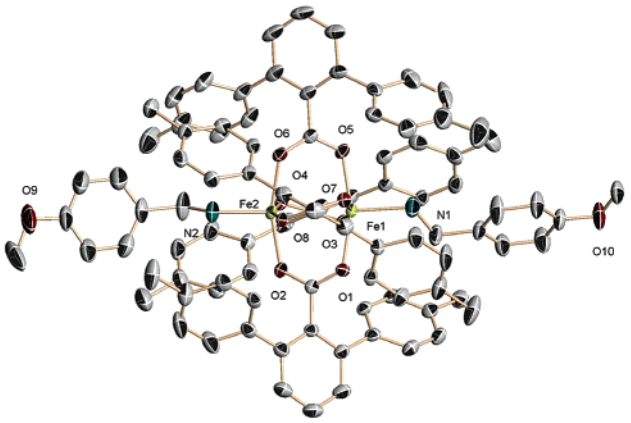

Figure 1. ORTEP drawing of **2** showing 50% probability thermal ellipsoids. CH_2Cl_2 solvent molecules and hydrogen atoms are omitted for clarity.

Scheme 2

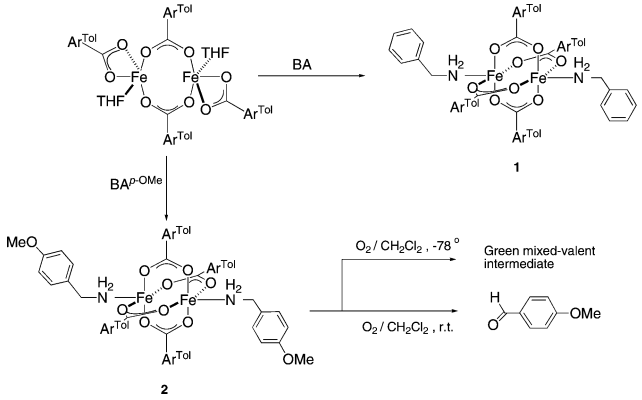

Table 1. Summary of Pertinent Structural and Physical Characterization Data for $[Fe_2(\mu\text{-}O_2CAr^{Tol})_4(BA)_2]$ (**1**), $[Fe_2(\mu\text{-}O_2CAr^{Tol})_4(BA^{p-OMe})_2]$ (**2**), and the Related $[Fe_2(\mu\text{-}O_2CAr^{Tol})_4(4\text{-}^tBuC_5H_4N)_2]$ (**3**) Compounds

	1	**2**	**3**
Fe···Fe distance (Å)	2.7937(6)	2.7638(17)	2.8229(9)
δ (mm/s)	1.08(2), 1.12(2)	1.06(2), 1.14(2)	1.12(2)
ΔE_Q (mm/s)	2.12(2), 2.58(2)	2.12(2), 2.44(2)	3.05(2)
μ_{eff}/μ_B	7.8 (5 K)	8.6 (5 K)	≤1 (5 K)
	8.6 (65 K)	9.6 (15 K)	
	8.0 (300 K)	7.9 (300 K)	6.5(300 K)
$E_{1/2}$ vs NHE		770 mV	284 mV
ref	this work	this work	9, 13

coordinated to the metal in axial positions through pockets that are generated by the four bulky carboxylate ligands of the diiron center.

The zero-field Mössbauer spectra of solid samples of **1** and **2** at 4.2 K displayed isomer shift and quadrupole splitting parameters that are characteristic of high-spin iron(II) species (Table 1; Figures S2 and S3).[9,11,12] The effective magnetic moments (μ_{eff} values) (Figure 2, **2**; Figure S4, **1**) steadily increase from 7.9 μ_B at 300 K to a maximum of 9.7 μ_B at 15 K, before decreasing to 8.6 μ_B at 5 K. This behavior signals weak exchange coupling between the two high-spin iron(II) centers of the tetracarboxylate-bridged dimer. More work is necessary to derive the appropriate exchange coupling and

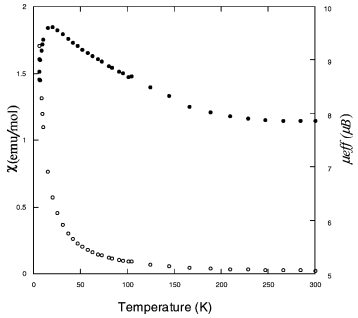

Figure 2. Plots of the temperature dependence of the effective magnetic moment (μ_{eff}) (●) and molar susceptibility (χ_M) versus temperature (○) for a solid sample of **2**. Data were recorded at an external magnetic field of 1 T.

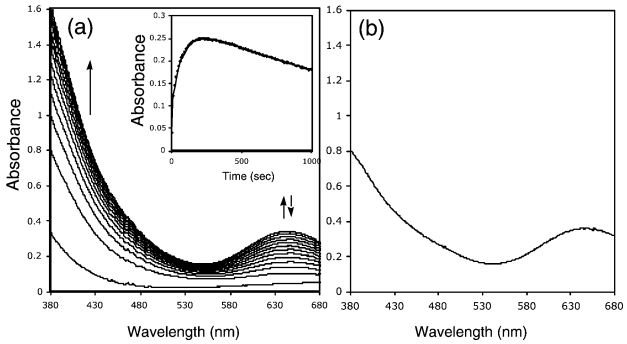

Figure 3. (a) Spectral changes that occur during the reaction of **2** (1.46 × 10^{-4} M**)** with excess dioxygen in CH_2Cl_2 at −78 °C. (Inset) Kinetic trace for the development and decay of the intermediate recorded at 645 nm. (b) UV−vis spectrum of $[Fe_2(\mu\text{-}O_2CAr^{Tol})_4(BA^{p-OMe})_2](PF_6)$ in CH_2Cl_2.

zero field splitting parameters. The significant difference between the magnetic behavior of **1** and **2** compared to that previously reported for the paddlewheel complex $[Fe_2(\mu\text{-}O_2CAr^{Tol})_4(4\text{-}^tBuC_5H_4N)_2]$[9] may reflect small differences (∼0.03−0.06 Å) in Fe···Fe distance as well as the electronic character of the axial ligands.

Since **1** is not very soluble in most aprotic organic solvents, further studies were performed exclusively with compound **2**. Cyclic voltammetry in CH_2Cl_2 solution revealed a quasi-reversible, one-electron oxidation ($E_{1/2}$ = 770 mV vs NHE; ΔE_p = 112 mV, scan rate = 25 mV/s) (Figure S5). When a CH_2Cl_2 solution of **2** was allowed to react with dioxygen at −78 °C, a green color developed (λ_{max} = 645 nm) over a period of 200 s. This metastable solution decayed within ∼6 h at −78 °C to form a yellow species (Figure 3). Clues to the identity of the green intermediate were provided by resonance Raman (rR) and EPR spectroscopic measurements. The frozen solution rR spectrum revealed no ^{18}O-sensitive bands, which indicates that the chromophore does not contain an Fe−O bond derived from dioxygen (Figure S6). The X-band EPR spectra of the green intermediate measured at 5 K exhibited two distinct signals at g = 12 and g = 2.0 (Figure 4). By analogy with previous work,[13] these results suggest that the broad g = 12 signal may originate from a high-spin Fe(II)Fe(III) unit with an $S = {}^9/_2$ ground state, the green intermediate thus being a ferromagnetically coupled $[Fe^{II,III}_2(\mu\text{-}O_2CAr^{Tol})_4(BA^{p-OMe})_2]^+$ cation. This assignment

(12) Drago, R. S. In *Physical Methods in Chemistry*; W. B. Saunders Company: Philadelphia, 1977; pp 530−551.

(13) Lee, D.; Pierce, B.; Krebs, C.; Hendrich, M. P.; Huynh, B. H.; Lippard, S. J. *J. Am. Chem. Soc.* **2002**, *124*, 3993−4007.

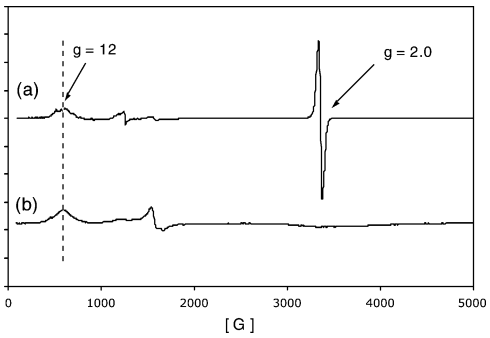

Figure 4. X-band EPR spectra of a frozen CH_2Cl_2 solution sample of (a) intermediate species generated by the oxygenation of **2** at −78 °C and (b) $[Fe_2(\mu\text{-}O_2CAr^{Tol})_4(BA^{p-OMe})_2](PF_6)$, measured at 5 K.

was confirmed by both the UV−vis and EPR spectra of the chemically synthesized, mixed-valent $[Fe_2(\mu\text{-}O_2CAr^{Tol})_4(BA^{p-OMe})_2](PF_6)$ complex (Figures 3b and 4b). The $g = 2.0$ signal (Figure 4) would then arise from an antiferromagnetically coupled Fe(III)Fe(IV) unit with an $S = {}^1/_2$ ground state. These mixed valence products might form in the following scenario. Reaction of **2** with dioxygen affords a transient adduct [**2**−O_2] that never builds up, possibilities for which are as $Fe_2^{II,III}(O_2^-)$, $Fe_2^{III}(O_2^{2-})$, or $Fe_2^{IV}(O^{2-})_2$. On the basis of the $E_{1/2}$ value for oxidation of **2** measured electrochemically, outer-sphere electron transfer upon reaction with dioxygen to form $\{Fe_2^{II,III} + O_2^-\}$[14] is unlikely to occur, due to the low reduction potential of dioxygen ($O_2/O_2^- = -550$ mV vs NHE in CH_2Cl_2).[15] We therefore conclude that, although a transient [**2**−O_2] adduct must form, before this species builds up to any spectroscopically detectable concentration, it reacts rapidly with unconverted **2** to afford an equimolar mixture of the green mixed-valent $Fe^{II}Fe^{III}$ complex and the $Fe^{III}Fe^{IV}$ species. A similar sequence of reactions was proposed for the chemistry of $[Fe_2(\mu\text{-}O_2CAr^{Tol})_4(4\text{-}^tBuC_5H_4N)_2]$ with dioxygen.[13]

The products formed upon exposure a CH_2Cl_2 solution of **2** to dioxygen at ambient temperature as analyzed by GC-MS include anisaldehyde with an average yield of 26(7)%, based on Fe^{II}_2, corresponding to *N*-dealkylation of putative hydroxylation at the benzylic position. This supposition was confirmed by an experiment in which $[Fe_2(\mu\text{-}O_2CAr^{Tol})_4(\alpha\text{-}d_1\text{-}BA^{p-OMe})_2]$ in CH_2Cl_2 solution at −78 °C was oxidized to afford anisaldehyde and d_1-anisaldehyde in a ratio of ∼1:3 (Figure S7). This kinetic isotope effect is consistent with C−H bond cleavage in a product-forming step of the reaction, the benzyl substituent in **2** being positioned such that the C−H bonds to be activated are α to the metal-bound nitrogen atom.

Oxidative *N*-dealkylation of this kind may proceed by one-electron oxidation at the nitrogen atom followed by proton transfer and rebound (Scheme 1), stepwise oxygen recoil/rebound,[16,17] or by a concerted[18] mechanism.[6] The absence of a lone pair of electrons in the coordinated BA^{p-OMe} ligand eliminates electron transfer from nitrogen as the initiating step for the present reaction. Determining which of the remaining two pathways effects the *N*-dealkylation reaction and the nature of the diiron species, $Fe_2^{III}(O_2^{2-})$, $Fe_2^{IV}(O^{2-})_2$, or some as yet unconsidered possibility, responsible for it remain important objectives for future work.

Acknowledgment. This work was supported by Grant GM32134 from the National Institute of General Medical Sciences. Raman spectra were obtained at the George R. Harrison Spectroscopy Laboratory Raman Facilities supported by the NIH under the Biomedical Research Technology Program (P41RR02594) and by NSF Grant 0111370-CHE. We thank Dr. J. Kuzelka for assistance in acquiring the Mössbauer spectra and helpful discussions, and Prof. T. J. Smith, Ms. E. M. Nolan, and Dr. J. A. Gardecki for performing the resonance Raman experiments.

Supporting Information Available: Synthetic details, description of methods, crystallographic information about **1** and **2** (Tables S1−S10), Figure S1 showing ORTEP diagrams of **1**, Mössbauer, magnetic, and CV traces for **1** and **2** (Figures S2−S5), resonance Raman data (Figure S6), NMR spectra for the kinetic isotope effect measurement (Figure S7), and an X-ray crystallographic file (CIF). This material is available free of charge via the Internet at http://pubs.acs.org.

IC0350133

(14) Payne, S. C.; Hagen, K. S. *J. Am. Chem. Soc.* **2000**, *122*, 6399−6410.
(15) Peover, M. E.; White, B. S. *Electrochim. Acta* **1966**, *11*, 1061−1067.
(16) Vaz, A. D. N.; Coon, M. J. *Biochemistry* **1994**, *33*, 6442−6449.
(17) Baik, M.-H.; Newcomb, M.; Friesner, R. A.; Lippard, S. J. *Chem. Rev.* **2003**, *103*, 2385−2419.
(18) Bach, R. D.; Andrés, J. L.; Su, M.-D.; McDouall, J. J. W. *J. Am. Chem. Soc.* **1993**, *115*, 5768−5775.